ISBN: 978-3-95450-215-8 ISSN: 2226-0366 doi:10.18429/JACoW-LINAC2022-FR1AA04

# SARAF COMMISSIONING: INJECTOR, MEBT AND CHOPPER

A. Chance, D. Chirpaz, D. Darde, G. Desmarchelier, R. Duperrier, J. Dumas†,
G. Ferrand, A. Gaget, F. Gohier, F. Gougnaud, T. Joannem, V. Nadot,
N. Pichoff, F. Senee, C. Simon, N. Solenne, D. Uriot, L. Zhao,
Commissariat à l'énergie atomique et aux énergies alternatives, Gif-Sur-Yvette, France
S. Cohen, I. Gertz, N. Goldberger, H. Isakov, B. Kaizer, A. Kreisel, Y. Luner, I. Mardor, H. Paami,
A. Perry, I. Polikarpov, E. Reinfeld, J. Rodnitsky, I. Shmuely, A. Shor, Y. Solomon, N. Tamim,
R. Weiss-Babai, L. Weissman, T. Zchut, Soreq Nuclear Research Center, Yavne, Israel

*Abstract*

IAEC/SNRC (Israel) is constructing an accelerator facility, SARAF, for neutron production. It is based on a linac accelerating 5 mA CW deuteron and proton beam up to 40 MeV. As a first phase, IAEC constructed and operated a linac (SARAF Phase I), from which remains an ECR ion source, a Low-Energy Beam Transport (LEBT) line and a 4-rod RFQ. Since 2015, IAEC and CEA (France) are collaborating in the second phase, consisting in manufacturing of the linac (Fig. 1). The injector control-system has been recently updated and the Medium Energy Beam Transport (MEBT) line has been installed and integrated to the infrastructure. It has been partially commissioned during the first semester of 2022. This paper presents the results of the integration, tests and commissioning of the injector and MEBT, before delivery of the cryomodules.

## INTRODUCTION

The Medium Energy Beam Transport (MEBT) is about 5 m long and includes 3 rebunchers and 8 quadrupoles. Each quadrupole was equipped with a steerer for orbit correction. The main objectives of this MEBT are to:

- adapt the beam coming from the RFQ to the Linac,
- clean transverse halo if necessary: possibilities to add 3 sets of slits and a chopper,
- minimize the residual gas going to the Superconducting Linac (SCL), and
- measure the beam characteristics: current, position, phase, energy, transverse and longitudinal profiles and emittances.

The MEBT was first assembled and preliminary tests were conducted at CEA Saclay mostly during the first semester of 2020. A dedicated test stand was built for checking alignment, vacuum, cooling, power supplies and the associated control systems. The MEBT arrived in Israel in August of 2020, to be installed and integrated by SNRC teams in its final position between the RFQ and a D-plate already used during Phase I [1] for the purpose of the MEBT commissioning. Two periods of commissioning with beam at SNRC were scheduled in Dec. 2021, and from May-December 2022 in parallel with other activities.

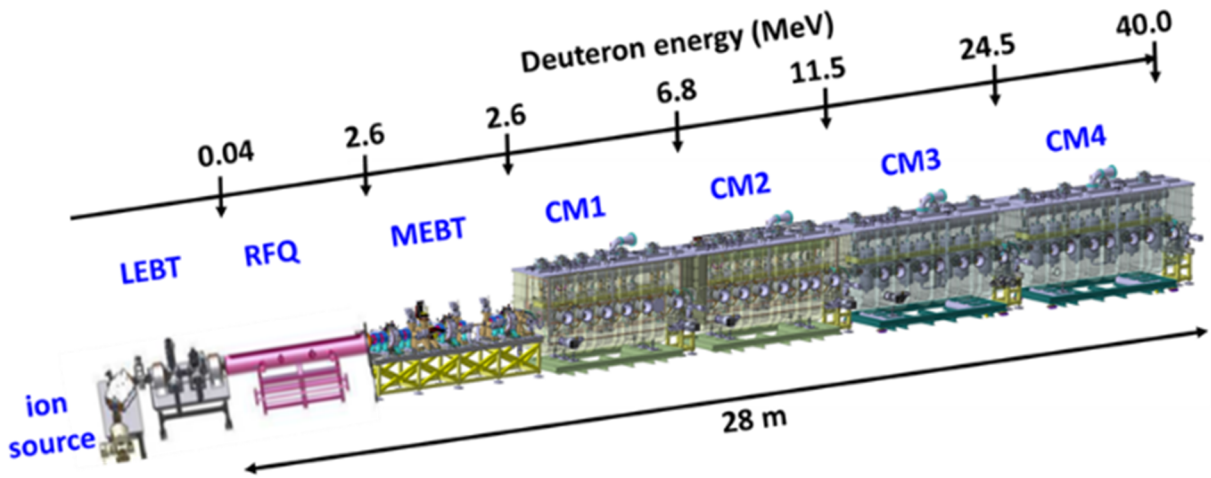


Figure 1: SARAF-LINAC.

† jonathan.dumas@cea.fr

ISBN: 978-3-95450-215-8 ISSN: 2226-0366 doi:10.18429/JACoW-LINAC2022-FR1AA04

## CONTROL SYSTEM

The SARAF Linac Control System is based on EPICS and MTCA.4, Siemens 1500 PLCs and Industrial PCs for the hardware architecture.
The software developments include the controls over:

- the magnetic element power-supplies,
- the cooling systems (water),
- the vacuum systems (pumps, valves),
- the cavity LLRF (including tuning motors),
- the beam diagnostics (BCMs, BLMs) electronics.

The EPICS IOCs are running on the MTCAs and IPCs. The MTCA platform is dedicated to fast acquisition and standardizes the very compact NATIVE-R2 crate with a common core on each crate: NAT-MCH-PHYS80 and RTM COMex-E3 boards and MRF boards for the timing system part (Fig. 2). For semi-fast and fast acquisition, a set of IOxOS boards has been added to this common platform and is used for current measurements and Beam Loss Monitors.

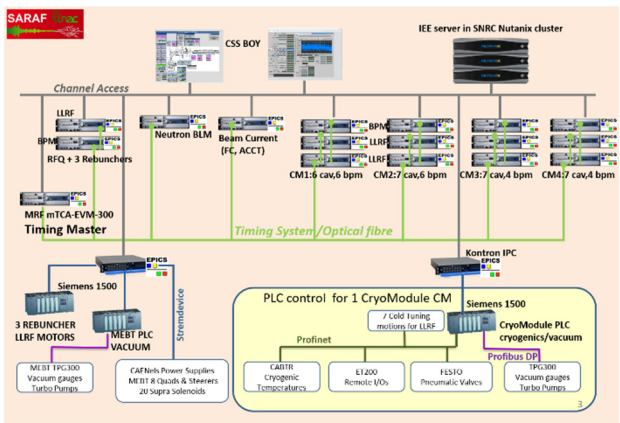


Figure 2: SARAF Linac Control System architecture [2].

The Injector including the RFQ was also updated with this common platform. An EPICS view of the injector system is presented in Fig. 3.

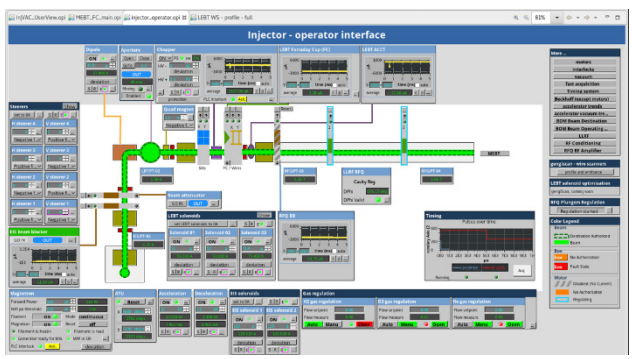


Figure 3: LCS injector view for accelerator operators.

Part of this development also includes local and global protection systems. As an example, a view of the SBCT, the Section Beam Current Transmission dedicated to shutting down the beam in case of harmful losses (see Fig. 4).

This application compares the current in 2 different ACCT, for the moment at the entrance and exit of the MEBT.

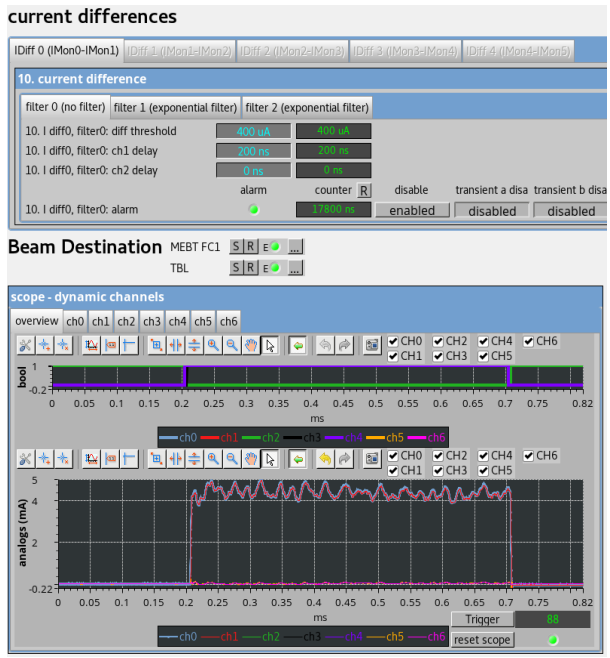


Figure 4: view of the SBCT.

## BEAM DIAGNOSTICS

For this commissioning phase, almost all the diagnostics are available and are represented in Fig. 5:

- 2 ACCT for current monitor, transmission and SBCT,
- 4 BPMs (Beam Position Monitor), for measuring the beam position and phase,
- 1 Fast Faraday Cup (FFC) in the first diagnostic box,
- 1 Faraday Cup at MEBT exit in the second diagnostic box

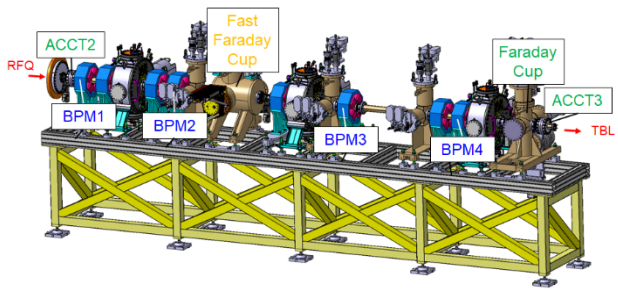


Figure 5: diagnostics and layout of the MEBT the 8 quadrupoles are in blue and red and the 3 rebunchers are in light grey.

The diagnostics are mostly for transmission, protection and longitudinal characterization of the beam. A SEM-Grid for transverse characterization will be integrated in the last semester of 2022. It will be located in the first diagnostic box. A system of three slits pairs is being prepared as well. A D-plate was connected after ACCT3, with some available diagnostics for longitudinal characterization (phase probes and FFC and a MPCT for current monitoring) as shown in Fig. 6.

ISBN: 978-3-95450-215-8 ISSN: 2226-0366 doi:10.18429/JACoW-LINAC2022-FR1AA04



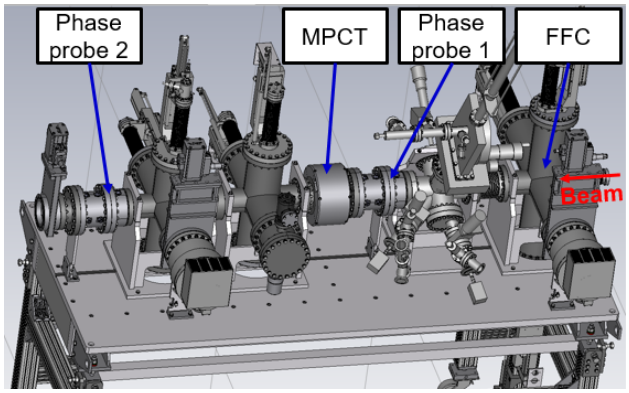


Figure 6: Available D-plate diagnostics [3].

## COMMISSIONING WITH BEAM

### *EIS Extraction Tuning*

Different ways of optimizing the source extraction voltage are studied using the RFQ and the MEBT diagnostics. The first method is the minimization of the fluctuations in the beam phase due to the synchrotron oscillation in the RFQ when varying the RFQ voltage as used at Spiral2 [4]. These fluctuations can be observed in Fig. 7 for 2 relatively "extreme" voltages compared to the nominal 20 kV.

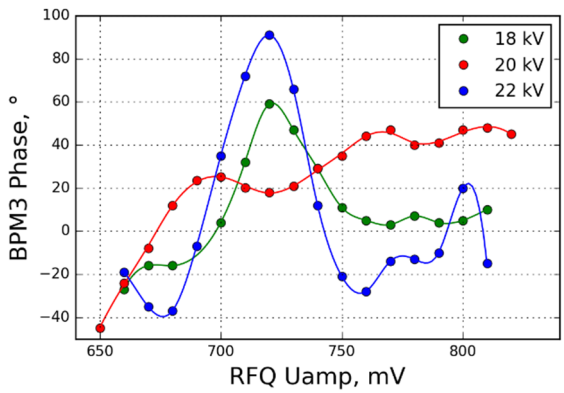


Figure 7: Beam phase measurement in one button of BPM3 (MEBT) as a function of the RFQ rod voltage for 3 source extraction voltages.

Another method to optimize the EIS voltage is to monitor the transmission on the Faraday Cup at the end of the MEBT (relatively to an ACCT located upstream of the RFQ), see Fig. 8. The nominal EIS voltage gives the highest transmission through the RFQ. The Toutatis/TraceWin simulation of a beam with a transverse emittance of 0.1 and 0.2 □.mm.mrad seems to be in a good lower and upper limit for the measurement and can indicate that the transverse emittance before the RFQ is of this order.

### *RFQ and MEBT Transmission Measurements*

The RFQ and the rebunchers were conditioned to the voltages required for proton operation using the new LLRF hardware and software [5]. The LEBT optics were adjusted to optimize the beam transmission at the RFQ exit. The

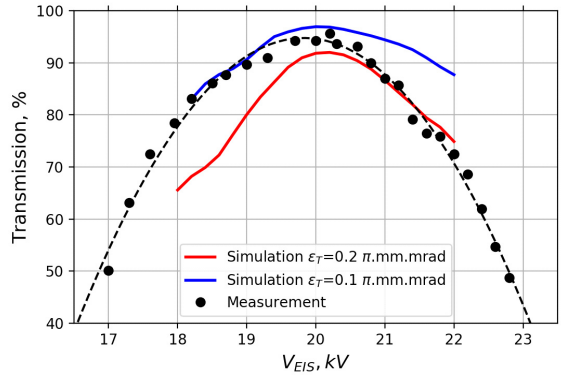


Figure 8: Beam transmission measurement (in black) on the FC at the end of the MEBT as a function of the beam injection energy. In blue and red, a TraceWin simulation of the beam transmission through the RFQ for a perfectly matched gaussian proton beam with a transverse emittance of 0.1 and 0.2 π.mm.mrad.

beam current was measured in the LEBT ACCT1 and in two different locations after the RFQ, in the ACCT2 right after the RFQ exit and in the FC at the end of the MEBT.The transmission as a function of the RFQ voltage (LLRF Uamp), presented in Fig. 9, shows that the transmission reaches a plateau for 710 mV (>90 %). From a transmission point of view, this voltage is the most efficient. The obtained RFQ transmission is significantly higher than reported during Phase I [6]. It is not clear yet the reason of such discrepancy. It might be attributed to improvements introduced at this stage to the SARAF ion source.

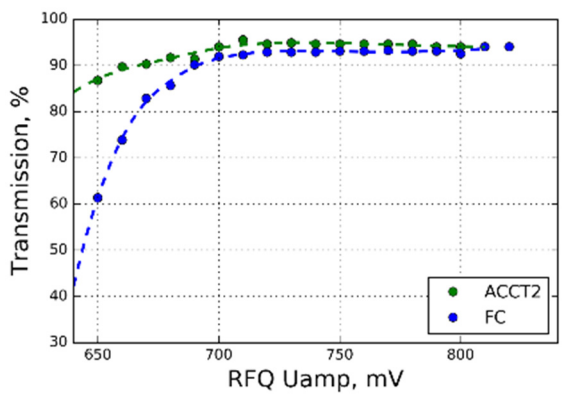


Figure 9: Beam transmission in ACCT2, in green, and the FC, in blue, of the MEBT as a function of the LLRF Uamp (RFQ voltage).

Transmission through the full MEBT was measured by comparison of ACCT2 and ACCT 3, while stopping the beam at the D-plate FC. The measurements yielded, practically, 100 % MEBT transmission. The MEBT optics was set according to the beam dynamics simulations for this measurement.

ISBN: 978-3-95450-215-8 ISSN: 2226-0366 doi:10.18429/JACoW-LINAC2022-FR1AA04

### *Beam Offset at RFQ Exit*

At the exit of the RFQ the beam was showing strong deviations and strong variations of the deviation as a function of the RFQ voltage, see Fig. 10. As the transverse diagnostics, namely the SEM-Grid, is not installed in the MEBT and the BPMs are not zeroed through beam based alignment, only the variation of the offset is really considered. Possibly the beam steering at the RFQ entrance should minimize this variation.

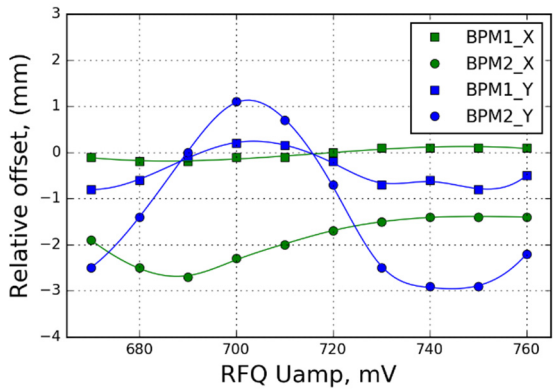


Figure 10: relative variation of the beam transverse offset (and angle) in the first 2 BPMs of the MEBT (optics off) as a function of the RFQ voltage.

### *Rebuncher Phasing*

The 2 BPM following each cavity are used as phase probes in order to tune the 3 rebunchers through the Signature Matching procedure [7]. The measurement (data) was very well matched with a cosine fit and TraceWin simulations. There was however, a discrepancy between the rebuncher's phase of no acceleration corresponding to an estimated energy of 1.28 MeV and the phase of the average estimated energy of the fit (1.287 MeV). This results in a 12° offset between the 2 points as seen in Fig. 11.

All the rebunchers have been tuned and present the same discrepancy. For the third rebuncher, the phase probes of the D-plates were used.

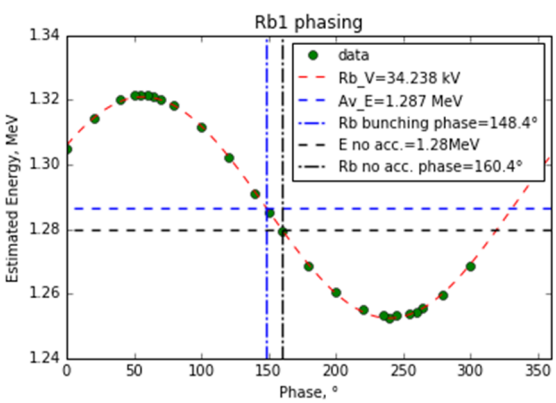


Figure 11: Rebuncher 1 phasing. In green is the estimated energy based on the measurement of the phase difference between BPM2 and 3. In red is the cosine fit. In black and blue are the discrepancy between the phase of no acceleration and the phase of the fit energy average.

### *Bunch Longitudinal Size Measurement*

The Fast Faraday Cup located after the first rebuncher measures the longitudinal bunch profile. The measured profile matches well the expected profile for simulations, see Fig. 12, but it can be improved by applying some filters to reduce noise or negative bouncing (at 50° for example) on the experimental waveform.

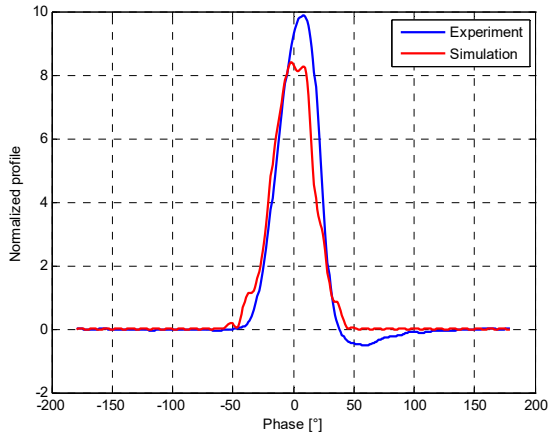


Figure 12: bunch longitudinal profile measured on the FFC after the first rebuncher in blue, and the TraceWin simulation in red.

### *Longitudinal Emittance*

The longitudinal emittance was calculated through the gradient variation method [8]. The bunch length was monitored on the MEBT FFC as a function of the rebuncher voltage (Fig. 13). A fast low-noise 6 GHz bandwidth amplifier, and 4 GHz scope were used in this measurements. The scope was placed next to the FFC, in order to minimize loss in the long cables.

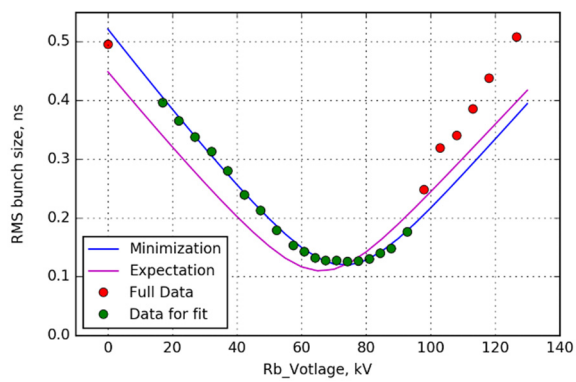


Figure 13: Emittance scan. Longitudinal bunch size measured on the FFC as a function of the rebuncher 1 voltage.

Depending on the rebuncher focalization, the longitudinal profile of the bunch can become distorted and for this reason the associated measurement was discarded for the emittance measurement. Two methods can be compared for calculating the emittance: (a) first order calculations (considering the rebuncher as a thin lens, neglecting space charge and a stable emittance) through the parabolic fit of

ISBN: 978-3-95450-215-8 ISSN: 2226-0366 doi:10.18429/JACoW-LINAC2022-FR1AA04



the square of the bunch size and (b) fitting the tracking simulations to the data through a minimization algorithm from the RFQ exit. The results can be seen on Table 1, after back tracking the emittance calculation for method (a) to the exit of the RFQ. Similar measurements were performed with the second FFC, placed at the beginning of the D-plate. In this case, the third rebuncher was used in this measurements. The results of this measurement was consistent with that presented in Table 1.

Table 1: Normalized RMS longitudinal emittance calculations at the RFQ exit (RFQ $U_{amp}$= 720 mV, $V_{EIS}$ = 20 kV)

| Proton (5 mA) | $\varepsilon_{\phi.w}$, π.deg.keV | $\alpha_{\phi.w}$ | $\beta_{\phi.w}$, deg/π.keV |
|---|---|---|---|
| Expectation | 50.46 | -0.01 | 1.43 |
| First Order (a) | 60.21 | -0.50 | 0.78 |
| Minimization (b) | 59.11 | -0.05 | 0.93 |

Several measurements of emittance in different conditions of the source extraction or RFQ voltage were studied after several weeks of shutdown and the installation of an additional amplifier [9] on rebuncher 1 (see Tables 2 and 3, respectively). These sets of measurements were done on the same day and show significant discrepancies between similar conditions of the injector which remain to be studied more extensively. A possible factor could be the adjustment of the transverse optics to maximize the beam current on the FFC.

Table 2: Normalized RMS longitudinal emittance calculations at the RFQ exit for different source voltage from the minimization method for protons (RFQ $U_{amp}$ = 710 mV)

| $V_{EIS}$ (kV) | $\varepsilon_{\phi.w}$, π.deg.keV | $\alpha_{\phi.w}$ | $\beta_{\phi.w}$, deg/π.keV |
|---|---|---|---|
| 19.2 | 46.05 | 0.15 | 0.84 |
| 20.0 | 47.73 | 0.33 | 1.11 |
| 21.1 | 56.10 | 0.44 | 1.24 |
| 22.0 | 65.08 | 0.41 | 1.73 |

Table 3: normalized RMS longitudinal emittance calculations at the RFQ exit in different conditions from the minimization method for protons ($V_{EIS}$ = 20 kV)

| RFQ $U_{amp}$, mV | $\varepsilon_{\phi.w}$, π.deg.keV | $\alpha_{\phi.w}$ | $\beta_{\phi.w}$, deg/π.keV |
|---|---|---|---|
| 680 | 77.39 | 0.69 | 1.84 |
| 710 | 76.43 | 0.86 | 1.03 |
| 740 | 61.49 | 0.24 | 0.86 |

## FAST CHOPPER

SNRC developed a fast chopper in the LEBT (see Fig. 14), to single out bunches [10]. It was achieved by fast sweep the beam along a collimator and letting just a small fraction into RFQ. The sweep HV pulse was synchronized with the accelerator RF. Figure 15 shows the difference between the two chopper modes (a) slow and (b) fast to select a so-called single bunch.

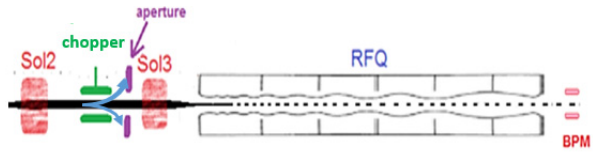


Figure 14: Layout of the SARAF chopper.

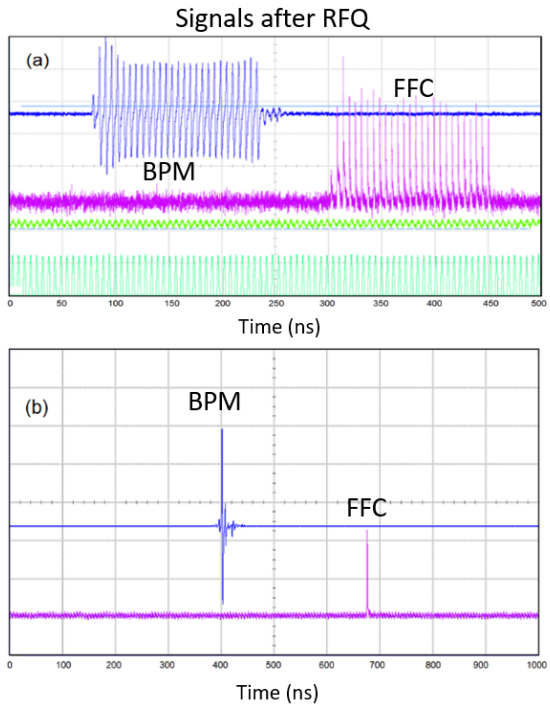


Figure 15: BPM and FFC signal after the RFQ (Phase I) using (a) the slow chopper mode and (b) the fast chopper mode.

## CONCLUSION

The MEBT was installed at SARAF, followed by its commissioning with and without beam. The feasibility of transporting a proton beam of 5 mA peak current was demonstrated and the main longitudinal characteristics were analysed. The commissioning will continue with the measurement of the beam transverse characteristics, the transport and characterization of the deuteron beam, the increase of beam power and finally the installation and commissioning of the cryo-modules.

## REFERENCES

[1] L. Weissman, "Diagnostics at SARAF", talk presented at Dapnia Lab., CEA Saclay, France, Oct. 2017, https://irfu.cea.fr/Phoea/file.php?class=std & file=Ast/file_1487_7_.pdf

[2] F. Gougnaud *et al.*., "Status of the SARAF-phase2 control system", in *Proc. ICALEPCS'21*, Shanghai, China, Oct. 2021, pp. 93-97. doi:10.18429/JACoW-ICALEPCS2021-MOPV001

[3] J. Rodnitski, private communication

[4] A. K. Orduz *et al.*, "Beam commissioning SPIRAL2", in *Proc. IPAC'21*, Campinas, Brazil, May 2021, pp. 2540-2543. doi:10.18429/JACoW-IPAC2021-WEXB05

ISBN: 978-3-95450-215-8 ISSN: 2226-0366 doi:10.18429/JACoW-LINAC2022-FR1AA04

[5] Orolia, https://orolia.com

[6] L. Weissman *et al*, "Installation, high-power conditioning and beam commissioning of the upgraded SARAF 4-rods RFQ'', *J. Instrum.*, vol. 13. p. T05004, 2018. doi:10.1088/1748-0221/13/05/T05004

[7] T. L. Owens, M. B. Popovic, K. Junck, T Kroc, and E. Mccrory "Phase scan signature matching for LINAC tuning", in *Proc. LINAC'94*, Tsukuba, Japan, Aug. 1994. pp. 893-895.

[8] P. Strehl, *Beam Instrumentation and Diagnostics*. Berlin, Springer, 2006.

[9] B. Kaizer *et al*., "High power solid state RF amplifiers for SARAF Phase II Linac", *Nucl. Instrum. Methods Sec. A*, vol. 1039, p. 167001, 2022. doi:10.1016/j.nima.2022.167001

[10] A. Shor *et al.,* "Fast chopper for single radio-frequency quadrupole bunch selection for neutron time-of-flight capabilities'', *Phys. Rev. Accel. Beams*, vol. 22, 2019. doi:10.1103/PhysRevAccelBeams.22.020403